processes

MDPI

Article

System Identification for Robust Control of an Electrode Positioning System of an Industrial Electric Arc Melting Furnace

Vicente Feliu-Batlle [1,*], Raul Rivas-Perez [2,*], Romar A. Borges-Rivero [2] and Roger Misa-Llorca [2]

[1] Escuela Técnica Superior de Ingeniería Industrial de Ciudad Real (ETSII), Universidad de Castilla-La Mancha (UCLM), 13071 Ciudad Real, Spain
[2] Departamento de Automática y Computación, Universidad Tecnológica de la Habana José Antonio Echeverría (CUJAE), La Habana 19390, Cuba; rabr774@gmail.com (R.A.B.-R.); rmisa@automatica.cujae.edu.cu (R.M.-L.)
* Correspondence: vicente.feliu@uclm.es (V.F.-B.); raul_rivas_perez@yahoo.es (R.R.-P.)

Abstract: Through system identification for robust control methods and utilizing real-time experimental field data, a comprehensive mathematical model is derived that represents the dynamic performance of a single electrode positioning system (EPS) in an industrial electric arc melting furnace (EAF). This EPS is characterized by large, time-varying dynamic parameters, which fluctuate based on operating conditions, specifically as the electrode weight changes within its operational range. The system identification methodology for robust control is developed in four main steps, progressing from experimental design to model validation. This approach yields a nominal model of the actual system and provides a trustworthy estimate of the region of uncertainty of the model, bounded by models of the real system under maximum and minimum electrode weight conditions (limit operating models). The methodology generates three fourth-order time-delay models using an ARMAX structure. The results are promising, as system identification for robust control enables the derivation of mathematical models specifically tailored for designing robust controllers. These controllers significantly enhance the EPS control system's performance and substantially reduce energy consumption and environmental emissions.

Keywords: system identification for robust control; electric arc melting furnace; electrode positioning system; nominal model; uncertainty model set; steelmaking industry

check for updates

Citation: Feliu-Batlle, V.; Rivas-Perez, R.; Borges-Rivero, R.A.; Misa-Llorca, R. System Identification for Robust Control of an Electrode Positioning System of an Industrial Electric Arc Melting Furnace. *Processes* **2024**, *12*, 2509. https://doi.org/10.3390/pr12112509

Academic Editor: Gorazd Karer

Received: 15 September 2024
Revised: 4 November 2024
Accepted: 7 November 2024
Published: 11 November 2024

Copyright: © 2024 by the authors. Licensee MDPI, Basel, Switzerland. This article is an open access article distributed under the terms and conditions of the Creative Commons Attribution (CC BY) license (https://creativecommons.org/licenses/by/4.0/).

1. Introduction

The steelmaking industry is one of the largest and most important globally, as it is a crucial driver of the world economy, with products indispensable for industrial development [1,2]. Due to the high global demand for steel, the industry is continually seeking to increase the efficiency of its manufacturing processes [3,4].

The steelmaking industry utilizes electric arc furnaces (EAFs) to generate the high temperatures required to melt steel scrap, typically between 1500 and 1550 °C [5,6]. The effective control of these furnaces is crucial, as operational improvements can lead to substantial energy savings and reductions in environmental pollution [7,8]. Figure 1 presents an image of an EAF.

Electrical energy is supplied to these furnaces via three massive graphite electrodes, each weighing up to several tenths of a ton, which are connected to the electricity network through a three-phase electrical transformer [9,10].

Electric arc furnaces consist of the following main systems [11,12]: (i) the power supply system, (ii) the thermal system, and (iii) the electrode positioning systems (EPSs). The EPSs are made up of three similar hydraulic actuator systems that control the vertical positioning of each electrode, along with the electrical measurement system [11].

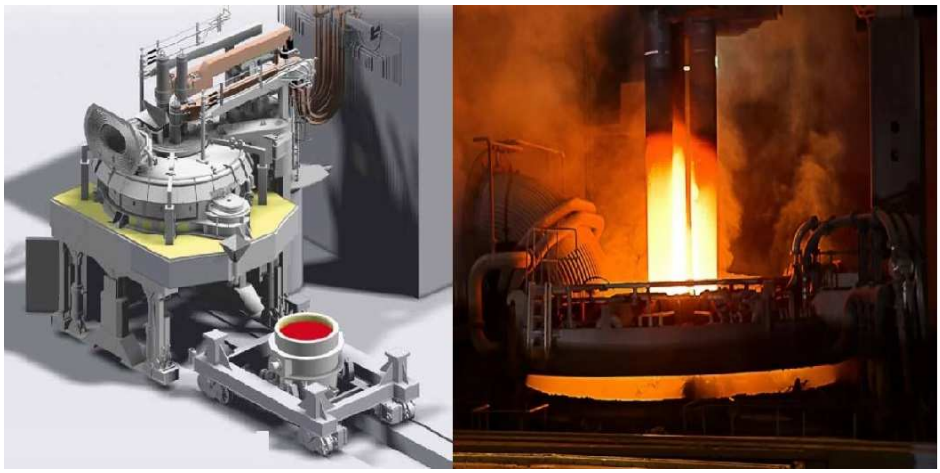


Figure 1. Picture of an EAF.

The electrical power required to melt the scrap depends on the lengths of the electric arcs, which are controlled by three distinct EPS controllers—one for each electrode—that operate similarly [13]. The primary objective of each EPS controller is to maintain a steady distance between the electrodes and the scrap [14,15]. Consistent arc lengths are desirable, as they imply a constant energy input, effectively transferring energy from the electrodes to the scrap [16].

In EPSs, the controlled variable is typically the arc impedance, which is directly proportional to the arc length [17]. Any deviation from the target arc impedance reduces the efficiency of energy usage [18,19]. EPS controllers are therefore essential, as they maintain the arc lengths—and consequently the arc impedances—at their reference values, ensuring a constant energy input to the scrap in EAFs [20]. It is well known that most EPS control systems in the steelmaking industry use simple PID controllers to regulate arc lengths [21–23].

Although EAFs are among the most energy-intensive industrial processes, a significant amount of energy is often lost due to inaccurate electrode positioning in many of them [24,25]. Consequently, efficient EAF operation requires the precise control of the EPSs [26,27].

EAFs are characterized by complex and uncertain nonlinear dynamic behaviors that can negatively impact power grid quality [28–30]. Additionally, the surface of the partially molten scrap moves continuously, altering its contour and introducing unmeasured random disturbances to the arc lengths [19]. To counter these disturbances, EPS controllers adjust the vertical position of the electrodes to maintain the required arc lengths [24]. Furthermore, the electrode weight also gradually decreases throughout the operating range [W_{max}, W_{min}] due to mass loss during the fusion process, leading to substantial time variations in the EPS dynamics [19,24]. Consequently, any mathematical model of this system must account for these time-varying parameters [31,32].

However, most controller design techniques are based on a nominal model, while the EPS's dynamic parameters vary with electrode mass consumption, resulting in a range of possible models (model uncertainty region) [33]. Therefore, EPS mathematical models must incorporate these parametric uncertainties.

Several studies have shown that single PID controllers may not be sufficiently effective for processes that exhibit complex dynamic behaviors [28–30], such as those with time-varying dynamic parameters [31–33]. Consequently, the currently installed PID controllers do not ensure successful EPS control, resulting in significant energy losses and environmental pollution [16,18,20].

Robust control is a powerful strategy for accurately managing processes with time-varying or uncertain dynamic parameters and disturbances [31]. Therefore, designing robust controllers for electrode positioning systems (EPSs) is of vital importance, as these

controllers enhance the performance of control systems. They also help reduce energy consumption and environmental contamination, while increasing the productivity and security of electric arc melting furnaces (EAFs) [32]. However, both the nominal model and the model uncertainty region are essential for the design of a robust controller for the EPS [33].

Owing to the complexity and severe operating conditions of electric arc furnaces (EAFs), a wide variety of models with diverse purposes, accuracy levels, and modeling procedures have been developed [10]. These range from basic models [3] to complex models [5]. For example, in studies [34–36], models were proposed based on physicochemical principles using mass and energy balance equations. In references [37,38], models were derived to forecast the power usage of EAFs. Models based on artificial neural networks were suggested in [39–42], while those founded on fuzzy logic were presented in [43,44]. Some linear models were developed using specific system identification procedures [45–48], which are generally sufficient to represent the major dynamic characteristics of the processes [49]. However, they do not necessarily have a physical interpretation; instead, they emphasize an accurate depiction of the true dynamics of the processes [48].

The main drawbacks of these models are that some do not accurately describe the dynamic behavior of EAFs. Others are characterized by their complexity, making them inadequate for controller design. Finally, while some models describe the nominal dynamic performance of EPSs, they fail to provide a consistent estimate of the model's uncertainty region. This uncertainty arises because, during the scrap melting process, the mass of the electrodes is consumed, resulting in a continuous decrease in their weights and generating significant time modifications in the dynamics of the EPS hydraulic actuators. Consequently, robust controllers cannot be designed using these models. It is noteworthy that developing a complete dynamic model (including both the nominal model and its model uncertainty region) for EPSs is a challenging task due to the complexity of these systems and the harsh conditions within the EAFs.

Furthermore, because EAFs are complex processes, obtaining experimental data on their dynamic behaviors is a challenging task. As a result, simulated data generated in laboratories are frequently used to derive mathematical models. This class of models is easier to obtain and analyze, providing more convenient results [50,51].

System identification for robust control (SIRC) has been a research field of growing interest since the 1990s [52–54]. One of its fundamental purposes is to obtain mathematical models from experimental data that are appropriate to design robust controllers [55]. To this end, the identification methodology must determine, besides a nominal model, a dependable estimate of the model's uncertainty region [55]. In this work, we develop a system identification procedure for the robust control of a single EPS in an EAF.

Note that complete dynamic mathematical models oriented towards the design of robust controllers for EPSs in electric arc smelting furnaces have not been reported in the literature.

The key scientific novelty of this paper is the derivation, for the first time ever, of a complete dynamic mathematical model of a single EPS, which includes both a nominal model and its model uncertainty region, by applying SIRC procedures. The derived region of uncertainty of the model is confined by the true EPS models under the maximum and minimum electrode weight operating regimes (models representing the electrode weight limit operating regimes). A significant issue for our work is the derivation of the region of uncertainty of the EPS nominal model, which allows for an accurate depiction of the dynamic behavior of this complex industrial process. The implications for the steelmaking industry are significant, as the derived complete dynamic mathematical model of the EPS enables the design of high-efficiency robust controllers for this process. They ensure the accurate control of the EPS and contribute to a substantial decrease in the energy expenditure and environmental pollutant gasses.

2. Materials and Methods

2.1. EAF Description

We studied the electric arc melting furnace (EAF) at Antillana de Acero in Havana. It is a three-phase AC EAF that has a power consumption of approximately 410 kWh/ton [56]. This EAF comprises three main systems: a power supply system (PSS), an Electric Arc System (EAS), and the EPS. Figure 2 illustrates this EAF.

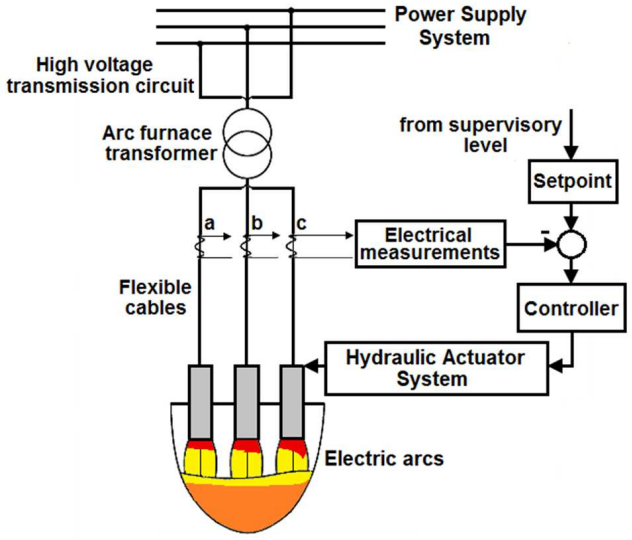


Figure 2. Schematic diagram of EAF.

The PSS is the source of energy for the EAF and consists of the high-voltage transmission circuit, the transformer that reduces the input voltage to the level required by the furnace, and the short net. The Electric Arc System (EAS) is responsible for the production of electric arcs, which occur when the electrodes are positioned over the slag, typically at a distance of approximately 10 to 15 cm from the slag [2]. The EPS comprises the hydraulic actuator system (HAS) and the electrical measurement system (EMS). The HAS includes a proportional control valve and a hydraulic cylinder. The structural diagram of the EPS is depicted in Figure 3.

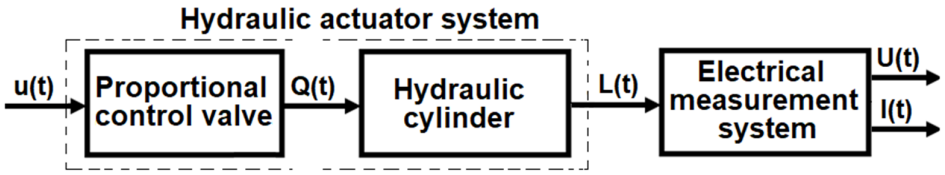


Figure 3. Diagram of the EPS.

Three similar HAS units are used to position the three graphite electrodes vertically, allowing for the regulation of the electric arc length according to the input voltage signal.

The hydraulic circuit primarily consists of a central reservoir, hydraulic pumps, a hydraulic tank, hydraulic cylinders, a secondary hydraulic source, and proportional control valves with a variation range of −10 V to 10 V. The working fluid is a water–glycol mixture, which is easy to handle and non-flammable. Each hydraulic cylinder operates the accessories attached to it, including the electrode arm, graphite electrode, and connecting cables, as well as cooling water. The hydraulic tank has a capacity of 7.2 m^3 and an operating pressure of 66 bar. The pumps operate within a pressure range of 0 to 220 bar and a flow rate of 0 to 0.0027 m^3/s. The specifications of the electrodes used are as follows: high-power electrodes (HPs) with a diameter of 400 mm, a length of 2400 mm, and a maximum weight of 550 kg.

Each electrode is placed independently with its own control system, which generates an input voltage signal for the proportional control valve that regulates the fluid flow from the hydraulic tank to the hydraulic cylinder. This signal enables the vertical motion of the electrode, adjusting the arc length and maintaining its arc impedance at a constant reference value. The piston of the hydraulic cylinder moves upward at maximum speed when the input voltage signal to the control valve is 10 V and downward when it is −10 V. The open-loop EPS control system diagram, featuring an arc impedance controller for a single phase, is illustrated in Figure 4.

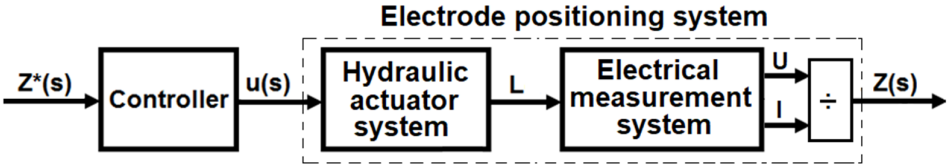


Figure 4. Diagram of the EPS control system for a single phase.

The electrical measurement system measures the voltage level and electric current of each phase in real time, sending these signals to the PLC, which calculates the arc impedance for use in controlling the EAF.

Various disturbances can cause fluctuations in the length of the electric arc. These include continuous displacements of the molten scrap's surface, variations in the scrap's conductance, and gas blowing. The controller adjusts the electrode position to mitigate these disturbances and keep a constant arc length.

The EPS control system is crucial because it directly adjusts the arc length and, consequently, its impedance by positioning the electrode. This system regulates the power input and resistance through arc impedance management in relation to the operating conditions.

Note that in arc impedance control, which is founded on keeping a constant arc length, the three EPS-controlled systems are generally decoupled [16]. Therefore, arc impedance control can be regarded as comprising three independent EPS controllers [16,17].

2.2. System Identification for Robust Control of EPS

The operational data of EPSs were readily available. However, the environment for data collection and experiment development in EAFs was particularly challenging due to the excessive dust and high temperatures associated with steelmaking.

The system input is the input voltage, denoted as u, and the output measurements, representing arc impedance, are denoted as y. The data collected up to the discrete time N are denoted:

$$Z^N = \{u(1), y(1), \ldots, u(N), y(N)\}$$

The proposed identification procedure for the real electrode positioning system (the true system), based on the collected input/output data [53], was as follows:

Step 1: Experiment design.

Step 2: Data collection, parameter estimation, and the validation of the true system's linear model (DPVLS) are performed under the nominal electrode weight operating conditions (nominal model).

Step 3: DPVLSs are performed under the boundary electrode weight operating conditions (the region of uncertainty of the model).

Step 4: Derivation of the uncertainty set of the system models, which consists of the nominal model and its associated uncertainty region.

This paper focused on using this algorithm to develop a mathematical model suitable for designing a robust controller for an EPS.

2.3. Experiment Design

The field experimental data were collected from an EPS in the Antillana de Acero electric arc melting furnace. The available measurements included the phase voltage U(t), phase current I(t), and input voltage signal u(t).

The PLC that controls the EAF calculates the arc impedance $Z(t)$ using the expression in [57,58]:

$$Z(t) = \frac{U(t)}{I(t)} \quad (1)$$

The EPS under study operated under different electrode weight regimes [16,56]. For the robust control system identification of the EPS, the primary operating regimes were the nominal electrode weight regime ($W(t) = W_{nom}(t) = 325$ Kg) and the electrode weight limit regimes: the maximum electrode weight regime ($W(t) = W_{max}(t) = 550$ Kg) and the minimum electrode weight regime ($W(t) = W_{min}(t) = 100$ Kg).

The range of variation for the electrode weight operating regimes of the EPS under study is therefore:

$$[W_{max}, W_{min}] = \{W(t) | 550 \geq W(t) \geq 100\} \quad (2)$$

with $W_{nom} \in [W_{max}, W_{min}]$.

The operating regime at the standard electrode weight was considered nominal, and the corresponding model was denoted the nominal model. When the EPS operated under different electrode weight regimes, the dynamic performance of the nominal system changed, resulting in model parametric uncertainties that were bounded by the electrode weight limit operating regimes.

The EPS model considered arc impedance $Z(t)$ as the output variable $y(t)$, and input voltage $u(t)$ as the input variable $u(t)$. The continuous movement of the surface of the molten steel scrap was treated as the main disturbance variable $v(t)$.

2.4. DPVLS Under the Nominal Electrode Weight Operating Regime

This step had two stages: nonparametric and parametric identification [59].

Nonparametric identification yields information about the dynamic characteristics of a process [59]. An initial experiment based on a step response was conducted to gather insights into the dynamic features of the process. Generally, this experiment provides valuable information about critical dynamic properties, such as time delays and model order [59]. The information obtained was subsequently utilized in the parametric identification to derive a model based on a more revealing experiment utilizing persistent excitation signals, such as a PRBS (pseudorandom binary sequence) [59].

As noted above, the nominal model of the true EPS is obtained at the nominal electrode weight of $W(t) = W_{nom}(t) = 325$ Kg.

2.4.1. Nonparametric Identification

The step response of the process was experimentally obtained. In this experiment, the control valve of electrode A was operated with a step command, while maintaining a stable 0 V signal (no movement) on electrodes B and C. The step command applied had a variation range of 10% (1 V) of the control valve's operating range.

The experiment was conducted within a temperature range of 1559 °C at the beginning to 1575 °C at the end. The initial arc impedance was 5.85 mΩ. Data corresponding to the variation in the arc impedance of electrode A, along with the growth of the magnitude of the input voltage, were recorded and stored in an industrial PC connected to the PLC that controls the EAF. The EPS response obtained is shown in Figure 5.

Results indicated that the dynamic performance of the EPS under the nominal electrode weight operating regime could be fitted to a time-delayed second- or higher order model. Additionally, the approximated values of the parameters of the nominal model were $K_{nom} = 4.25$ mΩ/V (static gain), $\tau_{nom} = 5$ s (time delay), and $t_{ss_nom} = 25$ s (settling time).

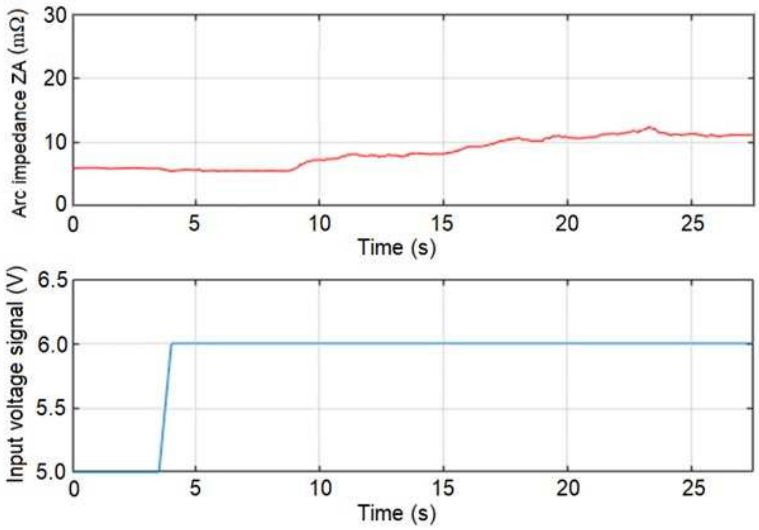


Figure 5. Step response of the EPS under the nominal electrode weight operating regime.

2.4.2. Parametric Identification

Parametric identification is the procedure developed to fit a model with a specified structure. This involves determining the order of the model structure and the values of its parameters that best match the data obtained through the experiment using a PRBS [59]. Parametric identification with binary sequences yields remarkably consistent estimates and confirms the time invariance of the models [60].

An experiment using a PRBS input command was also conducted to collect data with maximum information regarding the dynamic performance of the nominal electrode weight operating regime. The PRBS was designed to achieve a significant, albeit not excessive, variation in electrode positioning, leading to variations in arc impedance.

It was established that the PRBS must shift the magnitude of the input voltage signal to the control valve in periods that are multiples of 2 s, with an upper value of 10 s. This experiment involved applying a PRBS to the control valve of electrode A, enabling alternation between two input voltage levels representing a 10% variation (−1 V to 1 V) in the control valve's operating range. A stable 0 V signal (no movement) was maintained on electrodes B and C. The experiment was conducted within a temperature range of 1553 °C at the beginning to 1619 °C at the end. The initial arc impedance was 7.55 mΩ. The experimental field data corresponding to the variation in the arc impedance at electrode A, as well as the variation in the input voltage signal to the control valve, were sampled at intervals of 1 s. The total duration of this experiment was 312 s. The gathered data were stored on a computer and divided into estimation and validation data sets (left-hand and right-hand of the vertical red line, respectively). These are depicted in Figure 6.

The collected data were examined to verify their suitability for parameter estimation. The appropriateness of the data was confirmed, and, therefore, they were used.

The ARX, OE, and ARMAX model structures were evaluated to assess the most accurate representation of the dynamics of the nominal electrode weight operating regime. These structures are defined in [59]:

$$A(q)y_{ARX_nom}(t) = B(q)q^{-nk}u_{nom}(t) + \xi_{ARX_nom}(t) \quad (3)$$

$$y_{OE_nom}(t) = \frac{B(q)}{F(q)}q^{-nk}u_{nom}(t) + \xi_{OE_nom}(t) \quad (4)$$

$$A(q)y_{ARMAX_nom}(t) = B(q)q^{-nk}u_{nom}(t) + C(q)\xi_{ARX_nom}(t) \quad (5)$$

with $y_{ARX_nom}(t)$, $y_{OE_nom}(t)$, and $y_{ARMAX_nom}(t)$ being the outputs (with arc impedance being calculated from (1)) of the ARX, OE, and ARMAX models, labeled as j models, and

$$A(q) = 1 + a_1 q^{-1} + \ldots + a_{na} q^{-na} \quad (6)$$

$$B(q) = b_1 q^{-1} + \ldots + b_{nb} q^{-nb} \quad (7)$$

$$C(q) = 1 + c_1 q^{-1} + \ldots + c_{nc} q^{-nc} \quad (8)$$

$$F(q) = 1 + f_1 q^{-1} + \ldots + f_{nf} q^{-nf} \quad (9)$$

where na, nb, nc, nf represent the orders and a_i, b_i, c_i, f_i are the coefficients of the respective polynomials to be determined; nk denotes the system time delay; $\xi_{ARX_nom}(t)$, $\xi_{OE_nom}(t)$, and $\xi_{ARMAX_nom}(t)$ are uncorrelated random white noise sequences with zero mean for the ARX, OE, and ARMAX structures; and q is the discrete time shift operator ($q^{-1}u(k) = u(k-1)$).

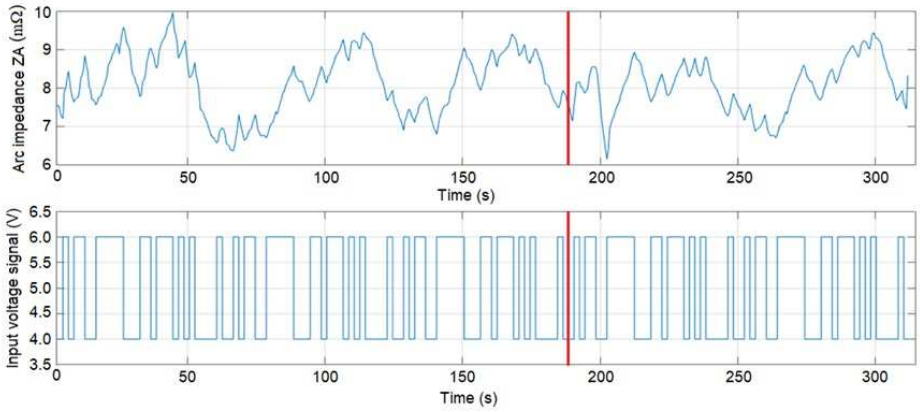


Figure 6. Experimental data of the response of the EPS to a PRBS under the nominal electrode weight operating regime.

The orders and coefficients of the model structures were determined using the estimation data set shown in Figure 6 and the MATLAB System Identification Toolbox R2024b. The vector $\theta_{N_nom\ j}$ of nominal parameters for the model structure j was identified using the Prediction Error Method (PEM), employing a least mean square criterion. This parameter vector was derived by [59]

$$\begin{aligned} \theta_{N_nom\ j} &= \arg\min_{\theta_{nom\ j}} \frac{1}{N} \sum_{t=1}^{N} \varepsilon_j^2(t,\ \theta_{nom\ j}) \\ &= \arg\min_{\theta_{nom\ j}} \frac{1}{N} \sum_{t=1}^{N} [y_{nom}(t) - y_{nom\ j}(t,\ \theta_{nom\ j})]^2 \end{aligned} \quad (10)$$

where $\varepsilon_j(t,\ \theta_{nom\ j})$ represents the prediction error, $y_{nom}(t)$ denotes the response of the nominal process, and $y_{nom\ j}(t,\ \theta_{nom\ j})$ signifies the output signal of the nominal model with the j structure, while N indicates the number of data points applied in the parametric identification ($N = 190$).

$\theta_{N_nom\ j}$ was identified for various polynomial orders, time delays, and sampling periods to derive the nominal model that most accurately described the data.

2.4.3. Model Validation

The cross-validation procedure [60] was used to validate the models, utilizing the field data set reserved for this purpose (122), as shown in Figure 6. This method is one of the most widely used approaches for model validation [59]. The most accurate model of the dynamics under the nominal electrode weight operating regime was determined by

calculating a precision index of the nominal models from the selected structures in relation to the validation field data. We used the FIT index as the precision index, which gives a measure of how well the model fits the data [59]:

$$\begin{aligned} \text{FIT} &= \left[1 - \frac{\|y-\hat{y}\|}{\|y-\overline{y}\|}\right] \times 100\% \\ &= \left[1 - \frac{\sum_{t=1}^{N} |y(t)-\hat{y}(t)|}{\sum_{t=1}^{N} |y(t)-\overline{y}(t)|}\right] \end{aligned} \tag{11}$$

where y is the measured output vector, $\hat{y}$ is the estimated output vector, and $\overline{y}$ is the mean of the output vector. Values of this index closer to 100% mean better models [59].

The variance of the residual error σ was also estimated. The residual error $\varepsilon(t)$ is the portion of the data that the model fails to reproduce. It provides insights into the model's accuracy and can be obtained using the expression [59]

$$\sigma = \frac{1}{N}\sum_{t=1}^{N} (\varepsilon(t) - \overline{\varepsilon})^2 \tag{12}$$

where

$$\varepsilon(t) = y(t) - \hat{y}(t) \tag{13}$$

$$\overline{\varepsilon} = \frac{1}{N}\sum_{t=1}^{N} \varepsilon(t) \tag{14}$$

The FIT and σ obtained from the derived models are exhibited in Table 1. It also includes the FIT and σ yielded by the second-order models of j structures.

Table 1. Validation results of the model of the nominal electrode weight operating regime.

Model Structure	Model Order (na, nb, nc, nd, nf, nk)	FIT	σ (mΩ)
ARX	(2, 2, 0, 0, 0, 2)	69.92%	$-1.2 < \varepsilon_{nom}(t) < 1.36$
OE	(0, 2, 0, 0, 2, 3)	70.86	$-1.1 < \varepsilon_{nom}(t) < 1.24$
ARMAX	(2, 2, 2, 0, 0, 5)	71.25%	$-0.6 < \varepsilon_{nom}(t) < 0.6$
ARX	(4, 4, 0, 0, 0, 3)	77.52%	$-0.45 < \varepsilon_{nom}(t) < 0.51$
OE	(0, 4, 0, 0, 4, 4)	83.46%	$-0.43 < \varepsilon_{nom}(t) < 0.37$
ARMAX	(4, 4, 4, 0, 0, 5)	87.31%	$-0.2 < \varepsilon_{nom}(t) < 0.2$

Table 1 illustrates that the highest FIT (87.31%) was achieved by the fourth-order nominal model using the ARMAX structure. The table also indicates that the lowest σ was obtained with the same model. This model is

$$\begin{aligned} y_{ARMAX_nom}(t) = {} & 0.3612y_{ARMAX_nom}(t-1) + 0.2721y_{ARMAX_nom}(t-2) \\ & -0.0717y_{ARMAX_nom}(t-3) + 0.02316y_{ARMAX_nom}(t-4) \\ & +0.0704u_{ARMAX_nom}(t-6) + 0.0912u_{ARMAX_nom}(t-7) \\ & +0.0020u_{ARMAX_nom}(t-8) + 0.0052u_{ARMAX_nom}(t-9) \\ & +\xi_{ARMAX_nom}(t) + 0.7332\xi_{ARMAX_nom}(t-1) + 0.6422\xi_{ARMAX_nom}(t-2) \\ & +0.8142\xi_{ARMAX_nom}(t-3) + 0.5321\xi_{ARMAX_nom}(t-4) \end{aligned} \tag{15}$$

The cross-validation results from expression (15) are exhibited in Figure 7. These results prove that the derived nominal model effectively describes the experimental data.

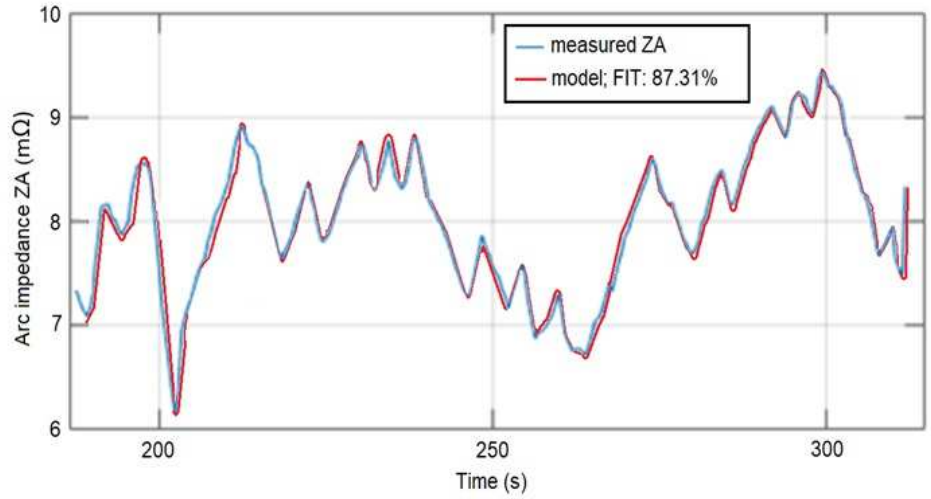


Figure 7. The cross-validation results of (15) under the nominal electrode weight operating regime.

The model (15) can be represented as a standard time-invariant linear model [60]:

$$y_{nom}(t) = G_{u_nom}(q,\ \theta)u_{nom}(t) + G_{v_nom}(q,\ \theta)e_{nom}(t) \tag{16}$$

where $G_{u_nom}(q,\ \theta)$ is the nominal transfer function from the discrete time input/output data, $u_{nom}(t)$, $y_{nom}(t)$, and $t = 1, 2, \ldots, N$, and θ_{nom} is the parameter vector; $G_{v_nom}(q,\ \theta)$ is the nominal noise transfer function parameterized by θ_{nom}, and $e_{nom}(t)$ is a nominal white noise sequence with zero mean.

The true EPS model, obtained under the nominal electrode weight operating regime from (17), can thus be denoted in the Laplace domain as [52]

$$G_{nom}(s) = [G_{u_nom}(s)\ \ G_{v_nom}(s)] \tag{17}$$

where

$$G_{u_nom}(s) = \frac{\Delta y_{nom}(s)}{\Delta u_{nom}(s)} = \frac{4.15}{(1.7s+1)(1.55s+1)(1.1s+1)(0.9s+1)}e^{-5s} \tag{18}$$

$$G_{v_nom}(s) = \frac{\Delta y_{nom}(s)}{\Delta v_{nom}(s)} = \frac{(0.9s+1)}{(1.5s+1)(1.4s+1)(s+1)(0.8s+1)} \tag{19}$$

2.5. DPVLS Under Electrode Weight Limit Operating Regimes (Model Uncertainty Region)

For system identification for the robust control of EPSs, knowledge of the variability of the parameters around the nominal model (i.e., the uncertainty region $\Delta G(s)$) is essential [59]. This is because robust control aims to provide a linear controller that stabilizes the feedback across the set $\Delta G(s)$ and optimizes performance in the worst-case scenario in the $\Delta G(s)$. Therefore, identifying the system's parameters under operating regimes at the minimum and maximum electrode weights is necessary.

2.5.1. Case of the Maximum Electrode Weight

As in Section 2.4.2, an experiment using a PRBS input command was conducted to collect data capturing the dynamic behavior of the maximum electrode weight operating regime, which occurred at $W(t)\ = W_{max}(t)\ = 525$ Kg.

This experiment involved applying a PRBS command to the control valve of electrode A, alternating between two input voltage levels (−1 V to 1 V) within the operating range of the valve. A stable 0 V signal (no movement) was maintained for electrodes B and C. The experiment took place within a temperature range of 1547 °C at the start to 1617 °C at the end, with an initial arc impedance of 7.20 mΩ.

The experimental field data corresponding to the variation in arc impedance at electrode A, as well as the variation in the input voltage signal to the control valve, were sampled at intervals of 1 s. The total duration of this experiment was 312 s. The data gathered were saved on a computer, filtered, and are presented in Figure 8.

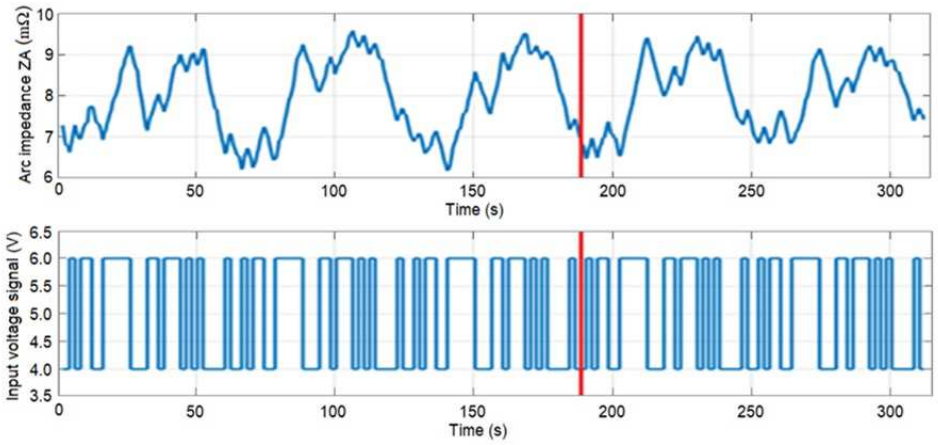


Figure 8. Experimental data of the response of the EPS to a PRBS under the maximum electrode weight operating regime. The red line separates the data used in the estimation from the data used in the validation.

Following a procedure similar to that in Section 2.4.2, we determined that the most accurate model was a delayed fourth-order model with the ARMAX structure

$$\begin{aligned} y_{ARMAX_max}(t) = {} & 0.2721 y_{ARMAX_max}(t-1) + 0.5312 y_{ARMAX_max}(t-2) \\ & -0.0638 y_{ARMAX_max}(t-3) + 0.0124 y_{ARMAX_max}(t-4) \\ & +0.0613 u_{ARMAX_max}(t-5) + 0.0562 u_{ARMAX_max}(t-6) \\ & +0.00413 u_{ARMAX_max}(t-7) + 0.0011 u_{ARMAX_max}(t-8) \\ & +\xi_{ARMAX_max}(t) + 0.0613 \xi_{ARMAX_max}(t-1) + 0.0562 \xi_{ARMAX_max}(t-2) \\ & +0.6241 \xi_{ARMAX_max}(t-3) + 0.5221 \xi_{ARMAX_max}(t-4) \end{aligned} \quad (20)$$

2.5.2. Model Validation

The cross-validation results for expression (20) on the validation data set are presented in Figure 9 and in Table 2, which also exhibits the obtained σ.

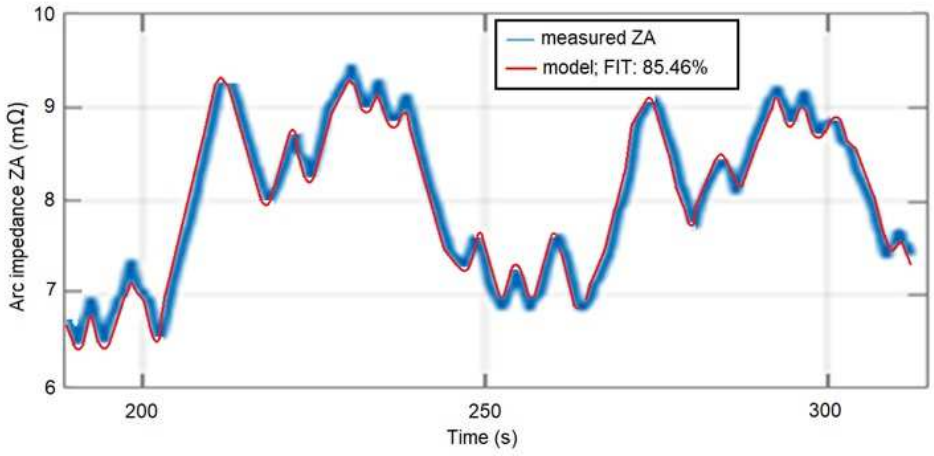


Figure 9. The cross-validation results of (20) under the maximum electrode weight operating regime.

Table 2. Validation outcomes of the models of the electrode weight limit operating regimes.

Electrode Weight Limit Operating Regimes	Model Order (na, nb, nc, nd, nf, nk)	FIT	σ (mΩ)
Maximum electrode weight operating regime	(4, 4, 4, 0, 0, 4)	85.46%	$-0.25 < \varepsilon_{max}(t) < 0.25$
Minimum electrode weight operating regime	(4, 4, 4, 0, 0, 6)	82.25%	$-0.3 < \varepsilon_{min}(t) < 0.3$

The model (20) is denoted in the Laplace domain as

$$G_{u_max}(s) = \frac{\Delta y_{max}(s)}{\Delta u_{max}(s)} = \frac{2.51}{(0.7s+1)(1.05s+1)(0.85s+1)(0.5s+1)} e^{-4s} \quad (21)$$

$$G_{v_max}(s) = \frac{\Delta y_{max}(s)}{\Delta v_{max}(s)} = \frac{(0.7s+1)}{(0.8s+1)(1.1s+1)(0.9s+1)(0.6s+1)} \quad (22)$$

2.5.3. Case of the Minimum Electrode Weight

A similar experiment to those conducted in Sections 2.4.2 and 2.5.1 was performed with a minimum electrode weight of $W(t) = W_{min}(t) = 100$ Kg.

This experiment was conducted within a temperature range of 1555 °C at the beginning to 1622 °C at the end. The initial arc impedance was 8.10 mΩ. The data collected were saved on a computer, filtered, and are presented in Figure 10.

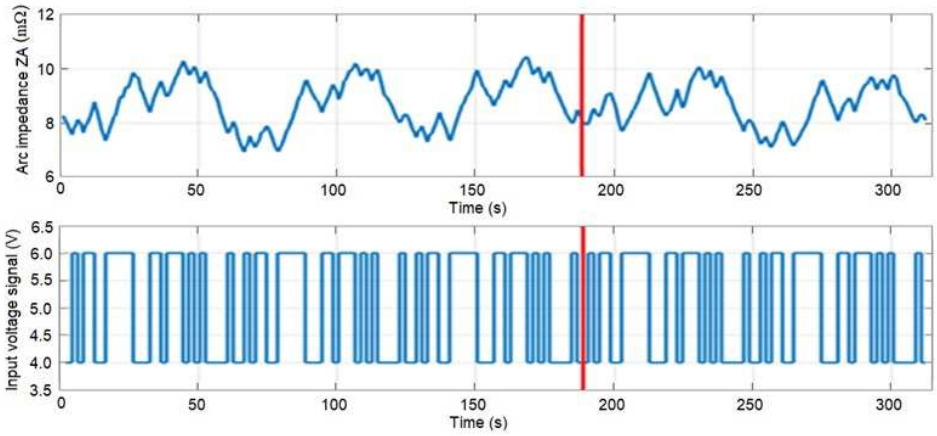


Figure 10. Experimental data of the response of the EPS to a PRBS under the minimum electrode weight operating regime.

Following a procedure similar to that in Section 2.4.2, we determined that the most accurate model was a delayed fourth-order model with the ARMAX structure:

$$\begin{aligned} y_{ARMAX_min}(t) = {} & 0.4732 y_{ARMAX_min}(t-1) + 0.6321 y_{ARMAX_min}(t-2) \\ & -0.0823 y_{ARMAX_min}(t-3) + 0.0432 y_{ARMAX_min}(t-4) \\ & +0.0822 u_{ARMAX_max}(t-7) + 0.0743 u_{ARMAX_min}(t-8) \\ & +0.00823 u_{ARMAX_max}(t-9) + 0.0044 u_{ARMAX_max}(t-10) \\ & +\xi_{ARMAX_max}(t) + 0.8341 \xi_{ARMAX_max}(t-1) + 0.7241 \xi_{ARMAX_max}(t-2) \\ & +0.7621 \xi_{ARMAX_max}(t-3) + 0.3125 \xi_{ARMAX_max}(t-4) \end{aligned} \quad (23)$$

2.5.4. Model Validation

The cross-validation results for expression (23) on the validation data set are presented in Figure 11 and in Table 2, which also shows the obtained σ.

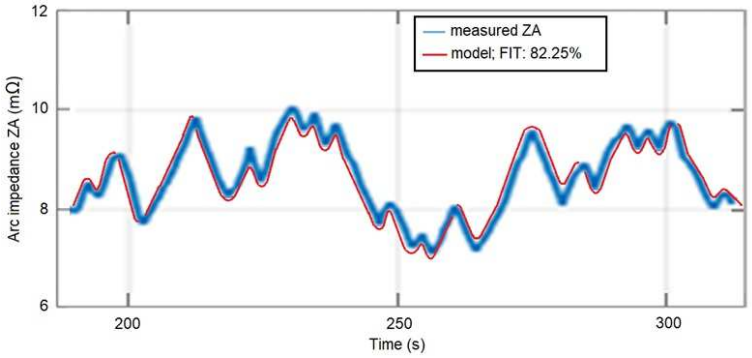


Figure 11. The cross-validation results of (23) under the minimum electrode weight operating regime.

The model (23) can be denoted in the Laplace domain as

$$G_{u_min}(s) = \frac{\Delta y_{min}(s)}{\Delta u_{min}(s)} = \frac{6.21}{(1.8s+1)(1.75s+1)(1.9s+1)(1.55s+1)} e^{-6s} \quad (24)$$

$$G_{v_min}(s) = \frac{\Delta y_{min}(s)}{\Delta v_{min}(s)} = \frac{(0.6s+1)}{(1.84s+1)(1.72s+1)(1.91s+1)(1.52s+1)} \quad (25)$$

3. Results

3.1. The Model Uncertainty Region of the True Electrode Positioning System

The weight of the electrodes of an EAF constantly decreases within the operating range $[W_{max}, W_{min}]$ because their mass is expended during the fusion process. Consequently, the parameters of their dynamic models experience large variations over time, as noted by several authors [16,17,19,20]. This leads to uncertainty in the accurate dynamic behavior of this system. These parametric uncertainties are bounded by the models of electrode weight limit operating regimes within the following ranges:

$$\begin{array}{l} K_{min} \le K(t) \le K_{max};\ T_{1\ min} \le T_1(t) \le T_{1\ max};\ T_{2\ min} \le T_2(t) \le T_{2\ max}; \\ T_{3\ min} \le T_3(t) \le T_{3\ max};\ T_{4\ min} \le T_4(t) \le T_{4\ max};\ \tau_{min} \le \tau(t) \le \tau_{max} \end{array} \quad (26)$$

Note that these uncertainty bounds were derived from experimental field data obtained from the Antillana de Acero EAF and statistical analysis.

Therefore, the region of uncertainty of the model of the EPS, $\Delta G(s)$, contains a set of models that includes the nominal model. This region is limited by the derived models corresponding to the minimum and maximum electrode weight operating regimes. The set of parameters that define this region is presented in Table 3.

Table 3. Obtained set of model uncertainties of the true EPS.

Model Uncertainty Set of the True EPS			
Model Parameters	**Nominal Electrode Weight Operating Regime Model**	**Bound of Uncertainty Region ΔG(s)**	
		Maximum Electrode Weight Operating Regime Model	**Minimum Electrode Weight Operating Regime Model**
K (mΩ/V)	$K_{nom} = 4.15$	$K_{min} = 2.51$	$K_{max} = 6.21$
T_1 (s)	$T_{1\ nom} = 1.70$	$T_{1\ min} = 0.70$	$T_{1\ max} = 1.80$
T_2 (s)	$T_{2\ nom} = 1.55$	$T_{2\ min} = 1.05$	$T_{2\ max} = 1.75$
T_3 (s)	$T_{3\ nom} = 1.10$	$T_{3\ min} = 0.85$	$T_{3\ max} = 1.90$
T_4 (s)	$T_{4\ nom} = 0.90$	$T_{4\ min} = 0.50$	$T_{4\ max} = 1.55$
τ (s)	$\tau_{nom} = 5.00$	$\tau_{min} = 4.00$	$\tau_{max} = 6.00$

Therefore, the set of EPS models is denoted as follows [52]

$$D = \{G_\Delta(s) | G_\Delta(s) = G_{nom}(s) + \Delta G(s)\} \quad (27)$$

3.2. Time-Domain Responses of the Set of the Uncertainty of the Models

The responses of the derived set of the uncertainty of the models of the EPS to step inputs, when the electrode weight shifts within the operating range [W_{max}, W_{min}], are shown in Figure 12.

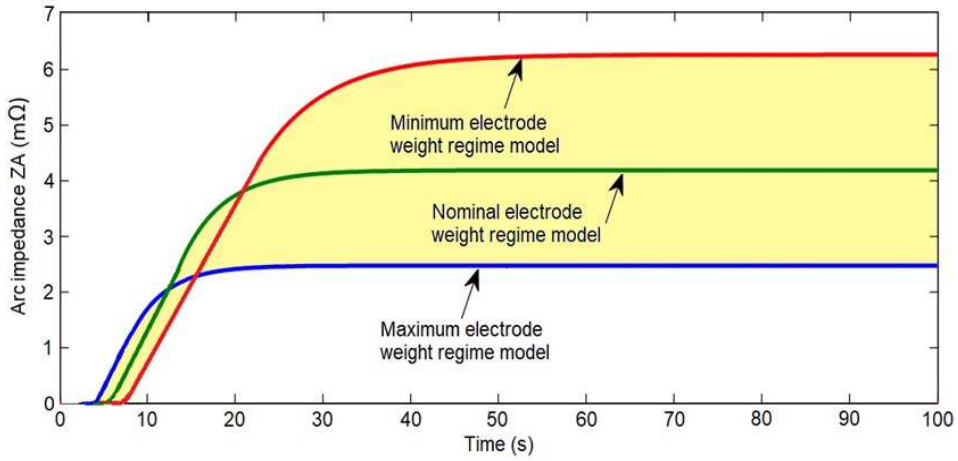


Figure 12. Step responses of the derived set of the uncertainty of the models of the EPS.

3.3. Frequency-Domain Responses of the Derived Set of the Uncertainty of the Models

The magnitude-phase diagrams (Bode plots) of the derived set of uncertainty models when the electrode weight shifts within the operating range [W_{max}, W_{min}] are shown in Figure 13.

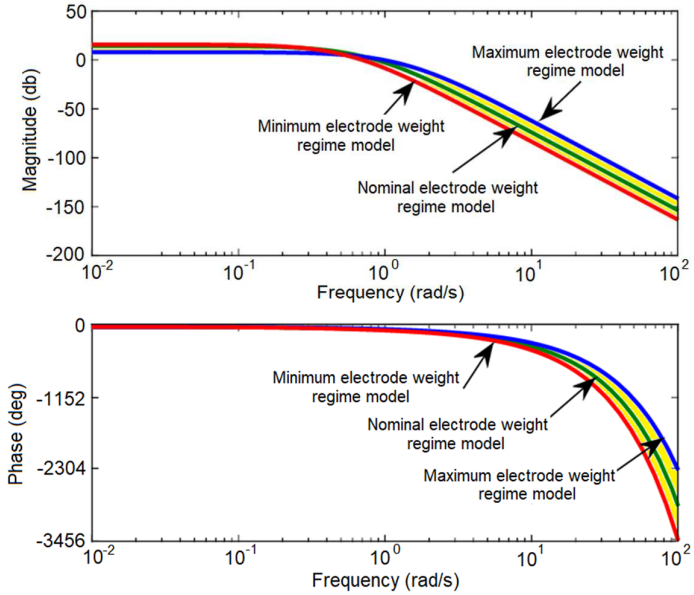


Figure 13. Bode diagrams of the derived model uncertainty set.

4. Discussion

The developed system identification procedure for robust control has significant scientific relevance, as it enables the derivation of both the nominal model and its region of uncertainty for a single EPS of an EAF.

The mathematical models previously reported focus solely on the nominal dynamic behavior of a single EPS and do not account for estimates of its uncertainty region, despite the significant time variations in the dynamic parameters of this process. This oversight arises from the constant decrease in the electrode mass within the operating range [W_{max}, W_{min}] during the melting process. Consequently, comprehensive dynamic mathematical models aimed at designing robust controllers for the EPS in an electric arc smelting furnace have not been reported in the literature.

Our procedure yields the nominal model of the EPS and its region of uncertainty when the EPS operates with electrode weights distinct from the nominal one (ranging between the minimum and maximum weights). The uncertainty bounds were derived from experimental field data obtained and statistical analysis.

Our procedure revealed that the most accurate model of the EPS dynamics is a delayed fourth-order linear ARMAX model structure. Fittings to the validation data set demonstrated that the derived transfer functions can accurately depict the true system's dynamic performance for data not included in the estimation process.

The proposed procedure, therefore, provides the system model uncertainty set (27), which includes the nominal model ($G_{nom}(s)$) and its uncertainty region ($\Delta G(s)$). The results obtained are valid and demonstrate that the developed system identification procedure for robust control yields an accurate model of a single EPS of an electric arc melting furnace.

It should be noted that the proposed identification procedure for robust control is the first step for implementing high-performance robust controllers for the EPSs of the Antillana de Acero EAF. These controllers will be designed based on the class of models derived in this paper.

Therefore, the results obtained demonstrate that the stated objectives were met and can be expanded to develop mathematical models aimed at designing robust controllers for other industrial processes with complex dynamic behavior.

5. Conclusions

We have developed a system identification procedure aimed at the robust control of a single EPS of the Antillana de Acero EAF. This procedure provides the EPS model uncertainty set, composed of the EPS nominal model and its region of uncertainty. This model (27) represents a significant advance in addressing the complex challenges associated with designing a robust control system for the EPSs.

Robust controllers are inherently more complex than conventional controllers; however, they offer greater precision, resulting in the improved performance of the EPS control system. As a result, these controllers significantly reduce the consumption of energy and environmental pollution.

The newly derived complete mathematical model (27) describes the true dynamics of the EPS more precisely, enabling a better approach to the challenges inherent to the robust control of the steel melting process in EAFs.

Author Contributions: Conceptualization, R.R.-P. and V.F.-B.; methodology, R.R.-P. and V.F.-B.; software, R.A.B.-R. and R.M.-L.; validation, R.A.B.-R. and R.M.-L.; formal analysis, R.R.-P.; investigation, R.R.-P.; resources, V.F.-B.; data curation, R.A.B.-R. and R.M.-L.; writing—original draft preparation, R.R.-P. and V.F.-B.; writing—review and editing, R.R.-P. and V.F.-B.; visualization, R.M.-L.; supervision, R.R.-P.; project administration, R.R.-P.; funding acquisition, V.F.-B. All authors have read and agreed to the published version of the manuscript.

Funding: This work has been financially supported by the University of Castilla-La Mancha (Spain) and the European Social Fund (FEDER) under Project 2023-GRIN-34307.

Data Availability Statement: The data presented in this study are available on request from the corresponding author.

Conflicts of Interest: The authors declare no conflicts of interest.

Abbreviation

Abbreviation	Meaning
EAF	Electric Arc Melting Furnace
EPS	Electrode Positioning System
PID	Proportional Integral Derivative Controller
AC-EAF	Alternating Current Electric Arc Melting Furnace
PSS	Power Supply System
EAS	Electric Arc System
HAS	Hydraulic Actuator System
EMS	Electrical Measurement System
PRBS	Pseudorandom Binary Sequence
PC	Personal Computer
PLC	Programmable Logic Controller
ARX	Auto Regressive with Exogenous Input
ARMAX	Auto Regressive Moving Average with Exogenous Inputs
OE	Output Error Model
PEM	Prediction Error Method
FIT	Performance Index
SIRC	System Identification for Robust Control

References

1. Verdeja González, L.F.; Fernández González, D.; Verdeja González, J.I. *Operations and Basic Processes in Steelmaking*; Springer: Cham, Switzerland, 2021.
2. Karbowniczek, M. *Electric Arc Furnace Steelmaking*, 1st ed.; CRC Press: Boca Raton, FL, USA, 2021.
3. Odenthal, H.J.; Kemminger, A.; Krause, F.; Sankowski, L.; Uebber, N.; Vogl, N. Review on modeling and simulation of the electric arc furnace (EAF). *Steel Res. Int.* **2018**, *89*, 1700098. [CrossRef]
4. Dutta, S.K.; Chokshi, Y.B. *Basic Concepts of Iron and Steel Making*; Springer: Singapore, 2020.
5. Abadi, M.M.; Tang, H.; Rashidi, M.M. A review of simulation and numerical modeling of electric arc furnace (EAF) and its processes. *Heliyon* **2024**, *10*, e32157. [CrossRef] [PubMed]
6. Shyamal, S.; Swartz, C.L. Real-time energy management for electric arc furnace operation. *J. Process Control* **2019**, *74*, 50–62. [CrossRef]
7. Martynova, E.S.; Bazhin, V.Y.; Kharazov, V.G. Increasing the level of control and management of arc steel smelting furnaces. *IOP Conf. Ser. Mater. Sci. Eng.* **2019**, *537*, 032039. [CrossRef]
8. Saboohi, Y.; Fathi, A.; Skrjanc, I.; Logar, V. Optimization of the electric arc furnace process. *IEEE Trans. Ind. Electron.* **2019**, *66*, 8030–8039. [CrossRef]
9. Hernandez, J.; Onofri, L.; Engell, S. Modeling and energy efficiency analysis of the steelmaking process in an electric arc furnace. *Metall. Mater. Trans. B* **2022**, *53*, 3413–3441. [CrossRef]
10. Hay, T.; Visuri, V.V.; Aula, M.; Echterhof, T. A review of mathematical process models for the electric arc furnace process. *Steel Res. Int.* **2021**, *92*, 2000395. [CrossRef]
11. Tomažic, S.; Andonovski, G.; Škrjanc, I.; Logar, V. Data-driven modelling and optimization of energy consumption in EAF. *Metals* **2022**, *12*, 816. [CrossRef]
12. Nikolaev, A.; Povelitsa, E.; Kornilov, G.; Anufriev, A. Research and development of automatic control system for electric arc furnace electrode positioning. *Appl. Mech. Mater.* **2015**, *785*, 707–713. [CrossRef]
13. Feliu-Batlle, V.; Rivas-Perez, R.; Castillo-Garcia, F.J.; Rodriguez-Martinez, C.A. A robust fractional order controller for an EAF electrode position system. *IFAC Proc. Vol.* **2014**, *47*, 10670–10675. [CrossRef]
14. Kleimt, B.; Krieger, W.; Mier Vasallo, D.; Arteaga Ayarza, A.; Unamuno Iriondo, I. Model-based decision support system for electric arc furnace (EAF) online monitoring and control. *Metals* **2023**, *13*, 1332. [CrossRef]
15. Feliu-Batlle, V.; Rivas-Perez, R. Robust fractional-order controller for an EAF electrode position system. *Control Eng. Pract.* **2016**, *56*, 159–173. [CrossRef]
16. Nikolaev, A.A.; Tulupov, P.G. Electric arc furnace control system with smelting stage diagnostic function and adaptive non-linear impedance controller. In Proceedings of the International Conference on Industrial Engineering, Applications and Manufacturing, Sochi, Russia, 17–21 May 2021; pp. 581–585.
17. Li, Y.; Mao, Z.Z.; Wang, Y.; Yuan, P.; Jia, M.X. Model predictive control synthesis approach of electrode regulator system for electric arc furnace. *J. Iron Steel Res. Int.* **2011**, *18*, 20–25. [CrossRef]
18. Kozyra, J.; Lozynskyy, A.; Lukasik, Z.; Kusminska-Fijalkowska, A.; Kutsyk, A.; Kasha, L. Increasing the level of autonomy of control of the electric arc furnace by weakening interphase interactions. *Energies* **2023**, *16*, 8114. [CrossRef]
19. Li, L.; Mao, Z. A direct adaptive controller for EAF electrode regulator system using neural networks. *Neurocomputing* **2012**, *82*, 91–98. [CrossRef]

20. Janabi-Sharifi, F.; Jorjani, G. An adaptive system for modelling and simulation of electrical arc furnaces. *Control Eng. Pract.* **2009**, *17*, 1202–1219. [CrossRef]
21. Niu, S.S.; Xiao, D. *Process Control, Engineering Analyses and Best Practices*; Springer Nature: Cham, Switzerland, 2022.
22. Benitez, I.O.; Rivas, R.; Feliu, V.; Sanchez, L.P.; Sanchez, L.A. Fuzzy gain scheduled Smith predictor for temperature control in an industrial steel slab reheating furnace. *IEEE Lat. Am. Trans.* **2016**, *14*, 4439–4447. [CrossRef]
23. Rivas-Perez, R.; Feliu-Batlle, V.; Castillo-Garcia, F.J.; Benitez-Gonzalez, I. Temperature control of a crude oil preheating furnace using a modified Smith predictor improved with a disturbance rejection term. *IFAC Proc. Vol.* **2014**, *47*, 5760–5765. [CrossRef]
24. Balan, R.; Hancu, O.; Lupu, E. Modeling and adaptive control of an electric arc furnace. *IFAC Proc. Vol.* **2007**, *40*, 163–168. [CrossRef]
25. Klimas, M.; Grabowsk, D. Application of the deterministic chaos in AC electric arc furnace modeling. *IEEE Trans. Ind. Appl.* **2024**, *60*, 4978–4986. [CrossRef]
26. Lozynskyy, O.; Lozynskyi, A.; Paranchuk, Y.; Biletskyi, Y. Optimal control of the electrical mode of an arc furnace on the basis of the three-dimensional vector of phase currents. *Math. Model. Comput.* **2019**, *6*, 69–76. [CrossRef]
27. Dietz, M.; Grabowski, D.; Klimas, M.; Starkloff, H.-J. Estimation and analysis of the electric arc furnace model coefficients. *IEEE Trans. Power Deliv.* **2022**, *37*, 4956–4967. [CrossRef]
28. Astrom, K.J.; Hagglund, T. *Advanced PID Control*; ISA—The Instrumentation, Systems, and Automation Society: Pittsburgh, PA, USA, 2006.
29. Calderon Mendoza, E.M.; Rivas-Perez, R.; Sotomayor-Moriano, J.J. Design of an adaptive neuro-fuzzy controller of an irrigation main canal pool. *IEEE Lat. Am. Trans.* **2016**, *14*, 471–476. [CrossRef]
30. Rivas-Perez, R.; Sotomayor-Moriano, J.; Perez-Zuniga, C.G. Design of a multivariable GPC based on an industrial PC for control of a reverse osmosis unit of a pharmaceutical industry. *Rev. Mex. Ing. Quim.* **2016**, *15*, 259–273.
31. Mercorelli, P. Robust control as a mathematical paradigm for innovative engineering applications. *Mathematics* **2022**, *10*, 4399. [CrossRef]
32. Feliu-Batlle, V.; Rivas-Perez, R. Control of the temperature in a petroleum refinery heating furnace based on a robust modified Smith predictor. *ISA Trans.* **2021**, *112*, 251–270. [CrossRef]
33. Tacx, P.; de Rozario, R.; Oomen, T. Towards model order selection for robust-control-relevant system identification. *IFAC-Papers-OnLine* **2021**, *54*, 1–6. [CrossRef]
34. Jawahery, S.; Visuri, V.V.; Wasbo, S.O.; Hammervold, A.; Hyttinen, N.; Schlautmann, M. Thermophysical model for online optimization and control of the electric arc furnace. *Metals* **2021**, *11*, 1587. [CrossRef]
35. Logar, V.; Dovzan, D.; Skrjanc, I. Modeling and validation of an electric arc furnace: Part 1, heat and mass transfer. *ISIJ Int.* **2012**, *52*, 402–412. [CrossRef]
36. Opitz, F.; Treffinger, P. Physics-based modeling of electric operation, heat transfer, and scrap melting in an AC electric arc furnace. *Met. Mater. Trans.* **2016**, *47*, 1489–1503. [CrossRef]
37. Carlsson, L.S.; Samuelsson, P.B.; Jönsson, P.G. Using statistical modeling to predict the electrical energy consumption of an electric arc furnace producing stainless steel. *Metals* **2020**, *10*, 36. [CrossRef]
38. Gajic, D.; Savic-Gajic, I.; Savic, I.; Georgieva, O.; Gennaro, S.D. Modelling of electrical energy consumption in an electric arc furnace using artificial neural networks. *Energy* **2016**, *108*, 132–139. [CrossRef]
39. Klimas, M.; Grabowsk, D. Application of shallow neural networks in electric arc furnace modeling. *IEEE Trans. Ind. Appl.* **2022**, *58*, 6814–6823. [CrossRef]
40. Garcia-Segura, R.; Vázquez Castillo, J.; Martell-Chavez, F.; Longoria-Gandara, O.; Ortegón Aguilar, J. Electric arc furnace modeling with artificial neural networks and arc length with variable voltage gradient. *Energies* **2017**, *10*, 1424. [CrossRef]
41. Reinicke, A.; Engbrecht, T.N.; Schüttensack, L.; Echterho, T. Application of an artificial neural network for efficient computation of chemical activities within an EAF process model. *Metals* **2024**, *14*, 736. [CrossRef]
42. Moghadasian, M.; Alenasser, E. Modelling and artificial intelligence-based control of electrode system for an EAF. *J. Electromagn. Anal. Appl.* **2011**, *3*, 47–55.
43. Kozyra, J.; Lozynskyy, A.; Lukasik, Z.; Kusminska-Fijalkowska, A.; Kutsyk, A.; Kasha, L. Electric arc furnace electrode movement control system based on a fuzzy arc length identifier. *Energies* **2023**, *16*, 7281. [CrossRef]
44. Paranchuk, Y.; Shabatura, Y.; Kuznyetsov, O. The electrodes positioning control system for the electric arc furnace basing on fuzzy logic. In Proceedings of the IEEE International Conference on Modern Electrical and Energy Systems, Kremenchuk, Ukraine, 21–24 September 2021.
45. Mohseni, M.; Askari, M. System identification of electric arc furnace suction subsystem. In Proceedings of the 6th National Conference on New Technologies in Electrical and Computer Engineering, Isfaham, Iran, 13–14 December 2023.
46. Collantes-Bellido, R.; Gomez, T. Identification and modelling of a three-phase arc furnace for voltage disturbances simulation. *IEEE Trans. Power Del.* **1997**, *12*, 1812–1817. [CrossRef]
47. Yu, F.; Mao, Z. Recursive identification for electric arc furnace—Electrode regulator system. In Proceedings of the 36th Chinese Control Conference, Dalian, China, 26–28 July 2017; pp. 1989–1994.
48. Guého, D.; Singla, P.; Majji, M.; Juang, J.N. Advances in system identification: Theory and applications. In Proceedings of the 60th IEEE Conference on Decision and Control, Austin, TX, USA, 14–17 December 2021.

49. Rodriguez Vasquez, J.R.; Rivas Perez, R.; Sotomayor Moriano, J.; Peran Gonzalez, J.R. System identification of steam pressure in a fire-tube boiler. *Comput. Chem. Eng.* **2008**, *32*, 2839–2848. [CrossRef]
50. Pauna, H.; Willms, T.; Aula, M.; Echterhof, T.; Huttula, M.; Fabritius, T. Electric arc length-voltage and conductivity characteristics in a pilot-scale ac electric arc furnace. *Metall. Mater. Trans. B* **2020**, *51*, 1646–1655. [CrossRef]
51. Xue, B.; Yang, L.; Guo, Y.; Chen, F.; Wang, S.; Zheng, F.; Yang, Z. Design and construction of a laboratory-scale direct-current electric arc furnace for metallurgical and high-titanium slag smelting studies. *Metals* **2021**, *11*, 732. [CrossRef]
52. Gevers, M. Identification for control: From the early achievements to the revival of experiment design. *Eur. J. Control* **2005**, *11*, 335–352. [CrossRef]
53. Rivas-Perez, R.; Feliu-Batlle, V.; Castillo-Garcia, F.J.; Linares-Saez, A. Mathematical model for robust control of an irrigation main canal pool. *Environ. Model. Softw.* **2014**, *51*, 207–220. [CrossRef]
54. Slavov, T.; Kralev, J.; Petkov, P. Identification, uncertain modelling, and robust control of embedded systems. *Eng. Sci. Technol.* **2021**, *2*, 96–115.
55. Chen, J.; Gu, G. *Control Oriented System Identification*; Wiley Interscience: New York, NY, USA, 2000.
56. Rodriguez-Martinez, C.A.; Rivas-Perez, R.; Feliu-Batlle, V.; Castillo-Garcia, F. Fractional order control system of EAF of Antillana de Acero. In Proceedings of the X International Symposium on Automation, XIV Convention and International Fair Informatica'2011, La Habana, Cuba, 7–11 February 2011.
57. Tian, W.; Wang, L.; Yu, J.; Lv, Y.; Zhang, S.; Xu, Q.; Gao, B. A hybrid impedance matching network for underwater acoustic transducers. *IEEE Trans. Power Electron.* **2023**, *38*, 7622–7633. [CrossRef]
58. Yang, X.; Zhang, Z.; Xu, M.; Li, S.; Zhang, Y.; Zhu, X.F.; Ouyang, X.; Alù, A. Digital non-Foster-inspired electronics for broadband impedance matching. *Nat. Commun.* **2024**, *15*, 4346. [CrossRef]
59. Ljung, L. *System Identification. Theory for the User*; Prentice Hall: Upper Saddle River, NJ, USA, 1999.
60. Rivas-Perez, R.; Sotomayor-Moriano, J.; Pérez-Zuñiga, G.; Soto-Angles, M.E. Real-time implementation of an expert model predictive controller in a pilot-scale reverse osmosis plant for brackish and seawater desalination. *Appl. Sci.* **2019**, *9*, 2932. [CrossRef]

Disclaimer/Publisher's Note: The statements, opinions and data contained in all publications are solely those of the individual author(s) and contributor(s) and not of MDPI and/or the editor(s). MDPI and/or the editor(s) disclaim responsibility for any injury to people or property resulting from any ideas, methods, instructions or products referred to in the content.